Journal of Materials Chemistry A

Accepted Manuscript

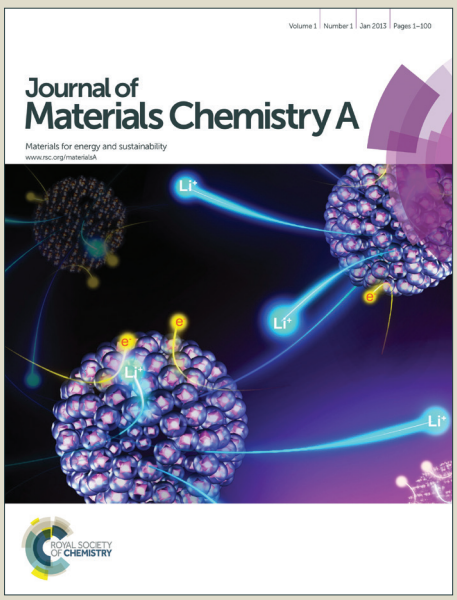

ROYAL SOCIETY OF CHEMISTRY

www.rsc.org/materialsA

Journal Name

RSCPublishing

ARTICLE

Interfacial architectures based on binary additive combination for high-performance Sn_4P_3 anodes in sodium-ion batteries

Cite this: DOI: 10.1039/x0xx00000x

Received 00th January 2012,
Accepted 00th January 2012

DOI: 10.1039/x0xx00000x

www.rsc.org/

Jun Yeong Jang,[a] Yongwon Lee,[a] Youngjin Kim,[b] Jeongmin Lee,[a] Sang-Min Lee,[c] Kyu Tae Lee,*[b] and Nam-Soon Choi*[a]

We demonstrate the important strategy to design suitable electrolyte systems that make the desirable interfacial structure to allow reversible sodiation/desodiation of Sn_4P_3 anodes. Our investigation reveals that the remarkable improvement in the electrochemical performance of Sn_4P_3 anodes for NIBs is achieved by the combination of fluoroethylene carbonate (FEC) with tris(trimethylsilyl)phosphite (TMSP). We clearly present unique functions of binary additive combination to build up a protective surface film on the Sn_4P_3 anode against unwanted electrolyte decomposition and to prevent the formation of the $Na_{15}Sn_4$ phase, which is accompanied by a large volume expansion during the Na insertion (sodiation) process.

Introduction

Sodium-ion batteries (NIBs) have recently gained recognition as an intriguing candidate for next-generation battery systems, largely on the basis of their similarities to lithium-ion batteries (LIBs) as well as the natural abundance of Na resources. Nevertheless, the practical application of NIBs is still quite challenging because NIBs face the critical problem of lower energy density than LIBs in terms of the cost per energy ($/Wh). To reduce the cost per energy unit of NIBs, electrode materials with high energy densities should be developed.[1-5] In addition, the Na ion has a larger ionic radius than the Li ion, which is a critical issue for the reversibility of Na insertion/extraction into/from Na host materials.

Extensive studies have been directed to improve the electrochemical properties of cathodes[6-11] and anodes[12-17] for high-performance NIBs. Among various anode materials, Sb-based (660 mAh g^{-1} for Na_3Sb)[12-14] and P-based (2596 mAh g^{-1} for Na_3P)[15,16] materials have been considered as Na-insertion anodes because of their high specific capacities. However, their electrochemical performance is unsatisfactory for ensuring long cycle life. Recently, Lee and co-workers reported Sn_4P_3 materials as promising anodes for NIBs.[18] The Sn_4P_3 anode materials exhibit a high reversible capacity of 718 mAh g^{-1} and a reasonably low redox potential of approximately 0.3 V vs. Na/Na^+, which is beneficial for the high operating voltage of a full cell.[18] The architecture of a stable and robust protective layer on the metallic anode is critically important to ensure good electrochemical performance of batteries, including NIBs.[19-21] Severe volume changes of the metallic anode due to Na insertion and extraction cause cracking of the anode particles and lead to a continuous solid electrolyte interphase (SEI)-filming process on the exposed active surface of the anode. Considerable SEI formation depletes the limited Na^+ source in a cell, results in thick SEI layers that induce a loss of electrical conduction pathways in the electrode, and causes poor cycling performance.[22-24] One of the efficient strategies for forming a stable artificial SEI layer on the metallic anode is the use of an reducible electrolyte additive. Recent studies for fluoroethylene carbonate (FEC) as a reducible additive have shown that the electrochemical performances of carbonaceous and metallic anodes in NIBs are greatly improved by the FEC-derived SEI layer.[17,19,25] Nevertheless, since the FEC-derived SEI layer mainly composed of highly resistive NaF may impede the sodiation/desodiation process of the anodes, a new class of electrolyte additives should be developed to achieve high-performance anodes in NIBs.

Herein, we propose a highly promising electrolyte additive combination that affords good cycling stability and improve the kinetic of desodiation of the Sn_4P_3 anodes. To understand the interfacial characteristics and electrochemical reactions of the Sn_4P_3 anodes with and without additives, observations of the surface morphology, and spectral and XRD studies of the Sn_4P_3 anodes were carried out. Moreover, unique functions of the binary additive in the interfacial architectures of the Sn_4P_3 anode are demonstrated.

Experimental

Preparation of electrolyte and electrode

The reference electrolytes used for the electrochemical tests of Sn_4P_3/Na cells were 1 M sodium perchlorate ($NaClO_4$, Aldrich, ≥ 98.0%) dissolved in a solvent mixture of ethylene carbonate (EC)/propylene carbonate (PC) (1/1, v/v). Solvents (Soulbrain Co., Ltd.) were used as received. 5 wt.% fluoroethylene carbonate (FEC, Soulbrain Co., Ltd) and 0.5 wt.% tris(trimethylsilyl) phosphite (TMSP, Aldrich) were introduced into the baseline electrolyte as functional additives. For the electrochemical tests, the Sn_4P_3 anode material was synthesized according to a procedure reported by our group.[18] The anode for the cell test consisted of a mixture of Sn_4P_3 active material, poly(acrylic acid) (PAA (M_w = 100,000), Aldrich), and super P carbon black for electronic conductivity enhancement (70:20:10 weight ratio) deposited onto a piece of Cu foil with a thickness of 18 μm. The resulting anodes were dried under vacuum at 110 °C for 2 h prior to being assembled into cells. To minimize the disintegrity of Sn_4P_3 anodes during cycling, the introduction of a mechanically stable binder, which accommodate severe volume changes and maintain electrical conduction network in the electrode, are needed. In this regard, we used PAA, which was proposed as an appropriate binder for anodes with large volume changes associated with the alloying and dealloying processes.[26]

Characterization

After being precycled, the cells were carefully opened in a glove box to retrieve their anodes. The anodes were rinsed in dimethyl carbonate to remove the residual $NaClO_4$-based electrolyte and then dried. To obtain XPS spectra and SEM images of Sn_4P_3 anodes, anodes retrieved from precycled cells were put on XPS and SEM sample holders in a glove box and the prepared samples were sealed under a vacuum by using an aluminum pouch film. All samples were stored in an aluminum pouch film before carrying out the XRD and SEM measurements and then, samples were rapidly transferred into chambers of XPS and SEM instruments to minimize any possible contamination. When the anodes were transferred from a pouch bag into a vacuum chamber of the XRD and SEM instruments, the samples were exposed to ambient conditions for 3 sec. The surface morphology of the anodes was observed using a field-emission scanning electron microscope (FE-SEM; JEOL JSM-6700F). During the SEM observations, an energy-dispersive X-ray spectrometer (EDS) was also used to determine the chemical components in the region under investigation. Ex situ X-ray photoelectron spectroscopy (XPS, Thermo Scientific K-Alpha system) measurements were performed on the dried anodes using Al-Kα (hν = 1486.6 eV) radiation under ultrahigh vacuum. XPS spectra were collected using a 0.10 eV step and an 80 eV pass energy. X-Ray diffraction (XRD) data on the anodes were obtained using a Rigaku D/MAX2500V/PC powder diffractometer equipped with a Cu-Kα radiation source (λ = 1.5405 Å); the samples were scanned over the 2θ range of 10-80°. Cell impedances of 2032 coin-type half-cells (Sn_4P_3 anode/metallic sodium) were monitored through AC complex impedance analysis with an IVIUM frequency response analyzer over a frequency range of 10 mHz to 1 MHz.

Electrochemical measurements

Galvanostatic charge and discharge cycling (WonATech WBCS 3000 battery measurement system) was performed with a two-electrode 2032 coin-type half-cell at 30 °C. Precycle and cycling tests of cells were performed in a potential window from 0 V to 1.5 V vs. Na/Na^+ at rates of C/20 and C/10, respectively.

Results and discussion

Electrochemical performance of Sn_4P_3 anodes with and without binary additive

Figs. 1a-c show the voltage profiles of Sn_4P_3/Na half-cells with and without functional additives (FEC and TMSP) for the precycle at a rate of C/20, and 1st, 5th, and 10th cycles at a rate of C/10. The baseline electrolyte delivers a relatively high Na insertion capacity of 1131 mAh g^{-1} compared with the FEC-added (720 mAh g^{-1}) or FEC+TMSP-added (852 mAh g^{-1}) electrolyte, as presented in Figs. 1a-c. This relatively high Na-insertion capacity of the Sn_4P_3 anode with the baseline electrolyte is attributed to the voltage plateau at approximately 0 V vs. Na/Na^+, which is also observed for the first 10 cycles in Figs. 1a-c.

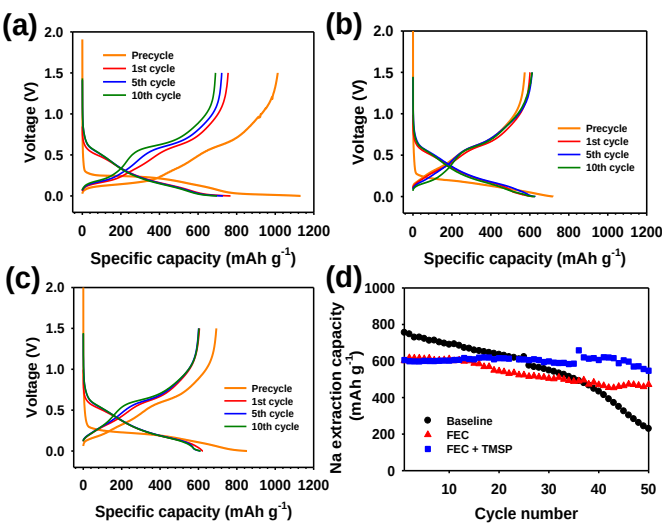

Fig. 1 Voltage profiles of the Sn_4P_3 anodes cycled in (a) baseline, (b) FEC-added, and (c) FEC+TMSP-added electrolytes at 30 °C. (d) Na extraction capacity of the Sn_4P_3 anodes at a rate of C/10. Precycle was performed at a rate of C/20 and a C/10 rate was applied for subsequent cycles.

Although the Sn_4P_3 anode with the baseline electrolyte delivered a high Na insertion capacity at the precycle, its reversible capacity was drastically decreased from 1131 mAh g^{-1} to 755 mAh g^{-1} in the 1st cycle (Fig. 1a). An initial Coulombic efficiency (ICE) of the Sn_4P_3 anode with the FEC+TMSP-added

electrolyte was slightly improved to 81.2%, compared with the FEC-added electrolyte (79.6%) at the precycle. This result is most likely because the TMSP additive modified the surface chemistry produced by the FEC additive. The Sn_4P_3/Na half-cell with the baseline electrolyte, which clearly exhibited the voltage plateau at approximately 0 V vs. Na/Na^+, delivered a Na extraction capacity of approximately 755 mAh g^{-1} during the 1st cycle, and its capacity gradually decreased during the first 10 cycles, as shown in Fig. 1a. After 30 cycles, severe capacity fading was observed for the Sn_4P_3 anode with the baseline electrolyte (Fig. 1d). The Sn_4P_3 anodes with FEC- or FEC+TMSP-added electrolyte exhibited Na extraction capacities of 600 mAh g^{-1} and 605 mAh g^{-1} during the 1st cycle, respectively, and their capacity was maintained during the first 10 cycles (Figs. 1b,c). A comparison of the Na extraction capacity of Sn_4P_3 anodes through 50 cycles clearly indicates that superior cycling stability was attained with the FEC+TMSP-added electrolyte compared to the baseline and FEC-added electrolytes (Fig. 1d). This result suggests that the formulation of FEC with TMSP additive leads to superior electrochemical reversibility of the Sn_4P_3 anode. On the contrary, the Sn_4P_3 anodes with only TMSP additive delivered discernibly reduced discharge (Na extraction) capacity and inferior cycling stability compared to the anodes with baseline electrolyte (Fig. S1). This implies that the use of TMSP additive does not make a desirable SEI layer on the Sn_4P_3 anode in absence of FEC additive.

Electrochemical reaction mechanism of Sn_4P_3 anodes with and without binary additive

The appearance of a voltage plateau at approximately 0 V (ii peak) in the baseline electrolyte is more clearly depicted in the dQ/dV graphs in Figs. 2a,d.

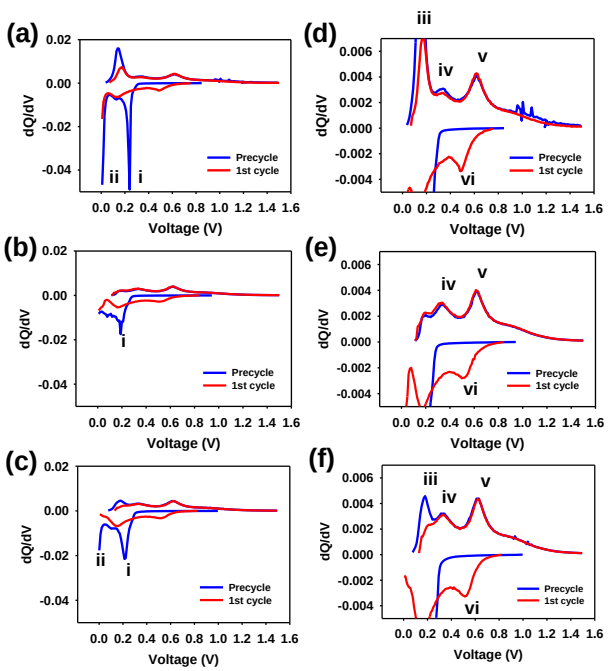

Fig. 2 Differential capacity plots (dQ/dV) of the precycle and the 1st cycle in (a,d) baseline, (b,e) FEC-added, and (c,f) FEC+TMSP-added electrolytes.

The Sn_4P_3 anode with FEC-added electrolyte showed no ii peak at approximately 0 V vs. Na/Na^+ during Na insertion at precycle (Fig. 2b). A considerably reduced ii peak appeared for the FEC+TMSP-added electrolyte (Fig. 2c). To understand the difference in the dQ/dV graphs for the Sn_4P_3 anodes with and without additives, the origin of the five main peaks (i to vi) at precycle must be discussed. During a sodiation process (Na insertion), the Sn_4P_3 anode can form three Na-Sn binary alloys corresponding to NaSn, Na_9Sn_4 and $Na_{15}Sn_4$ phases.[27] At approximately 0.2 V, corresponding to peak i during a sodiation process, the Sn_4P_3 is converted into NaSn, Na_9Sn_4 and Na_3P alloy materials ($Sn_4P_3 \rightarrow NaSn + Na_9Sn_4 + Na_3P$). At approximately 0 V (peak ii) during a sodiation process, Na-Sn-based alloy materials are converted into the Na_4Sn_{15} phase, which leads to severe volume expansion of the anode ($NaSn + Na_9Sn_4 + Na_3P \rightarrow Na_{15}Sn_4 + Na_3P$).[28] At approximately 0.15 V (peak iii) during a desodiation process (Na extraction), $Na_{15}Sn_4$ electrochemically oxidizes to form NaSn, Na_9Sn_4 and Na_3P phases prior to the desodiation of Na_3P phase ($Na_{15}Sn_4 + Na_3P \rightarrow NaSn + Na_9Sn_4 + Na_3P$). Two peaks at 0.3 V (peak iv) and 0.65 V (peak v) during a desodiation process reflect the desodiation of the NaSn, Na_9Sn_4 and Na_3P phases ($NaSn + Na_9Sn_4 + Na_3P \rightarrow Sn_4P_3$) (Fig. 2d-f).

As previously described, peak ii is closely linked to the formation of $Na_{15}Sn_4$, showing a huge volume expansion. To further confirm the origin of the ii peak observed in the baseline electrolyte, ex situ XRD patterns of the Sn_4P_3 anodes were collected before and after precycling, as shown in Fig. 3. Before precycling, the peaks corresponding to the crystalline phase of Sn_4P_3 are clearly shown in Fig. 3b. At a fully sodiated state, the broad peak corresponding to $Na_{15}Sn_4$ at 34° appeared for the Sn_4P_3 anode with the baseline electrolyte.[18] However, this broad peak was not observed for the FEC- and FEC+TMSP-added electrolyte (Fig. 3a), which means that the $Na_{15}Sn_4$ phase is readily produced in the baseline electrolyte, compared to the FEC- and FEC+TMSP-added electrolyte.

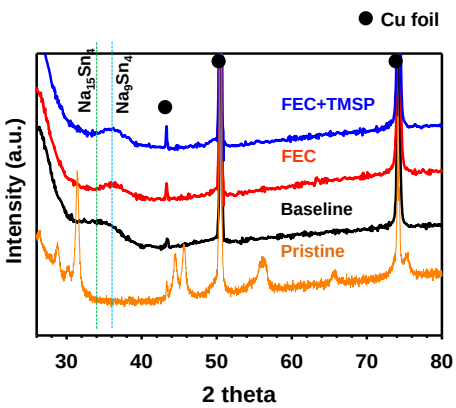

Fig. 3 Ex situ XRD pattern of Sn_4P_3 anodes after a full sodiation process in baseline, FEC-added, and FEC+TMSP-added electrolytes.

On the basis of the XRD studies, peak ii at approximately 0 V, which appeared for the baseline electrolyte, is believed to be strongly related to the formation of the $Na_{15}Sn_4$ phase during the sodiation process. Interestingly, the presence of FEC in the electrolyte led to the formation of Na_9Sn_4 rather than $Na_{15}Sn_4$, as shown by the XRD pattern in Fig. 3a. This result implies that the formation of the $Na_{15}Sn_4$ phase can be inhibited by the FEC additive.

Because this $Na_{15}Sn_4$ phase produced via further sodiation increases the capacity, the Sn_4P_3 anode with the baseline electrolyte could deliver a slightly higher Na insertion capacity (see Figs. 1a,d). However, severe volume expansion via the formation of the $Na_{15}Sn_4$ phase during the sodiation (Na insertion) process can result in agglomeration, cracking or pulverization of anode particles.[18] Indeed, the aggregation of anode particles between 1 and 2 m occurred after precycling in the baseline electrolyte, as shown in Figs. 5a,b. The size of the aggregated anode particles was greater than 3 m (Fig. 4b). In contrast, significant agglomeration of anode particles was not observed for the anode precycled in the FEC- and FEC+TMSP-added electrolytes (Figs. 4c,d). In particular, the anode precycled in the FEC+TMSP-containing electrolyte maintained the original morphology of its anode particles very well. This result suggests that good electrical connection in the anode with the FEC+TMSP binary additive is preserved during cycling. The superior cycling stability of the anode with the FEC+TMSP-added electrolyte can be explained by this maintained anode morphology.

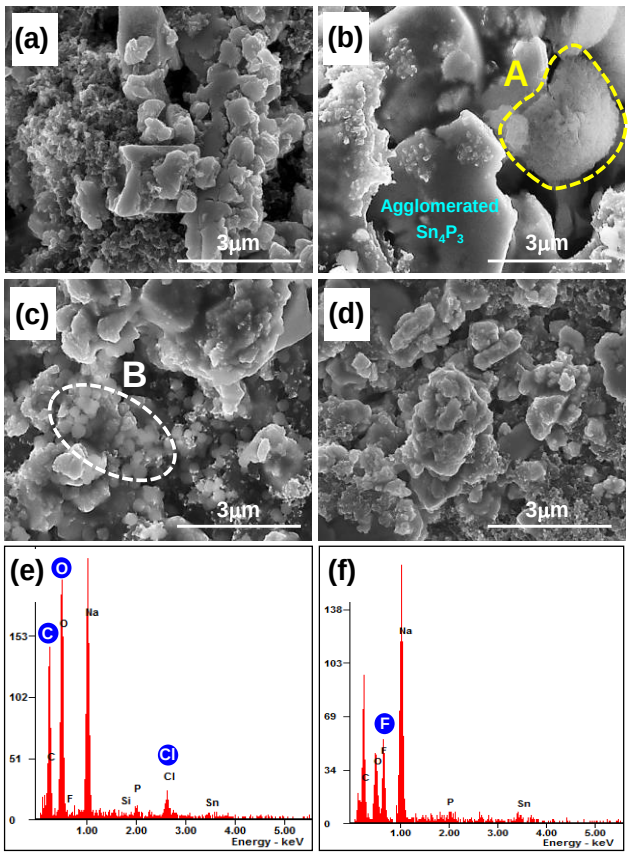

Fig. 4 The SEM images of (a) pristine Sn_4P_3 anodes and anodes precycled in (b) baseline electrolyte, (c) FEC-added electrolyte, and (d) FEC+TMSP-added electrolyte. The EDS spectra of Sn_4P_3 in (e) baseline electrolyte and (f) FEC-added electrolyte.

Moreover, the formation of a $Na_{15}Sn_4$ phase in the anode is not desirable because considerable volume changes cause continuous electrolyte decomposition on the newly exposed metallic anode surface through cracking, and thick solid electrolyte interphase (SEI) layers, which can impede the migration of Na ions into the anode, are thereby produced on the anode surface.

To identify the decomposition products formed on the Sn_4P_3 anode, energy-dispersive spectrometty (EDS) measurements were performed during the SEM observations (Figs. 4e,f). Zone A, selected from the anode precycled in the baseline electrolyte, exhibited pronounced carbon (C), oxygen (O), and chlorine (Cl) signals, which are produced by the unwanted decomposition of EC/PC solvents and ClO_4^- anions. These C, O, and Cl signals were detected not on the Sn_4P_3 anode particles but on carbon black particles, as shown in Fig. 4b. This result indicates that the electrolyte decomposition occurs on carbon black particles; thus, the decomposition byproducts protect the anode surface. For zone B, which was selected from the anode cycled in the FEC-containing electrolyte, a strong fluorine signal was resulted from FEC decomposition, and relatively weaker C, O, and Cl signals appeared (Fig. 4f). This result indicates that the FEC electrochemically reduces on the anode prior to the electrolyte decomposition and effectively suppresses the decomposition of solvents and salt.

Peak vi, which was not observed at precycle, is clearly seen for all electrolytes at the 1st cycle after precycling (Figs. 2d-f). The peak at 485 eV is assigned to the Sn metal, which can be formed via $NaSn + Na_9Sn_4 + Na_3P \rightarrow Sn + P + Sn_4P_3$.[29,30] It is noteworthy that Sn-based anodes suffers from severe capacity degradation due to the agglomeration of Sn particles during cycling.[18,28] Therefore, it is believed that the Sn_4P_3 with a relatively low fraction of the Sn metal during cycling ensure superior cycling performance. To investigate the influence of FEC and FEC+TMSP additives on the formation of the Sn metal, ex situ X-ray photoelectron spectroscopy (XPS) measurements of the Sn_4P_3 anodes after 20 cycles were performed.

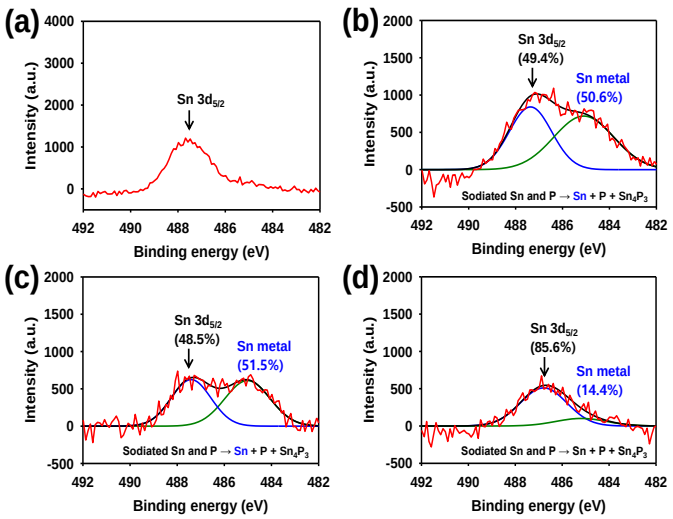

Fig. 5 Sn 3d XPS spectra of (a) pristine Sn_4P_3 anodes and after 20 cycles in (b) baseline electrolyte (c) FEC-added electrolyte and (d) FEC+TMSP-added electrolyte. The Sn-$3d_{5/2}$ peak corresponds to the Sn of the Sn_4P_3 anode material. The relative fraction of Sn metal produced during the desodiation was calculated by the peak fitting method.

Notably, the relative fraction of the peak corresponding to the Sn metal in the anodes cycled during 20 cycles in the FEC+TMSP-added electrolyte (14.4%) was dramatically reduced compared to the baseline (50.7%) and FEC-added

electrolytes (51.5%) (Figs. 5b-d). This finding suggests that the formation of the Sn metal in fully desodiated anode converted from the mixed phases of Na_xP and Na_ySn in the FEC+TMSP-added electrolyte is effectively inhibited. On the basis of the Sn 3d result for the anode after precycle, the vi peaks in the dQ/dV graphs of Figs. 2d-f are believed to be caused primarily by the sodiation reaction of Sn metal during Na insertion process. This resulting Sn metal, which was absent in the pristine Sn_4P_3 anode, undergoes electrochemical sodiation in subsequent cycles; thus, peak vi at approximately 0.5 V is expected to correspond to the sodiation of Sn metal.[17,28] Previously, the Yang group reported that Sn nanocrystals with low crystallinity are generated in the amorphous host matrix after the Na insertion/extraction process.[29]

Surface chemistry of Sn_4P_3 anodes with and without binary additive

Figs. 6g,h show that the peak assigned to NaF at approximately 685 eV is observed in the F 1s spectra of anodes cycled in the FEC- and FEC+TMSP-added electrolytes. NaF is believed to be formed by the FEC decomposition at the anode.[25]

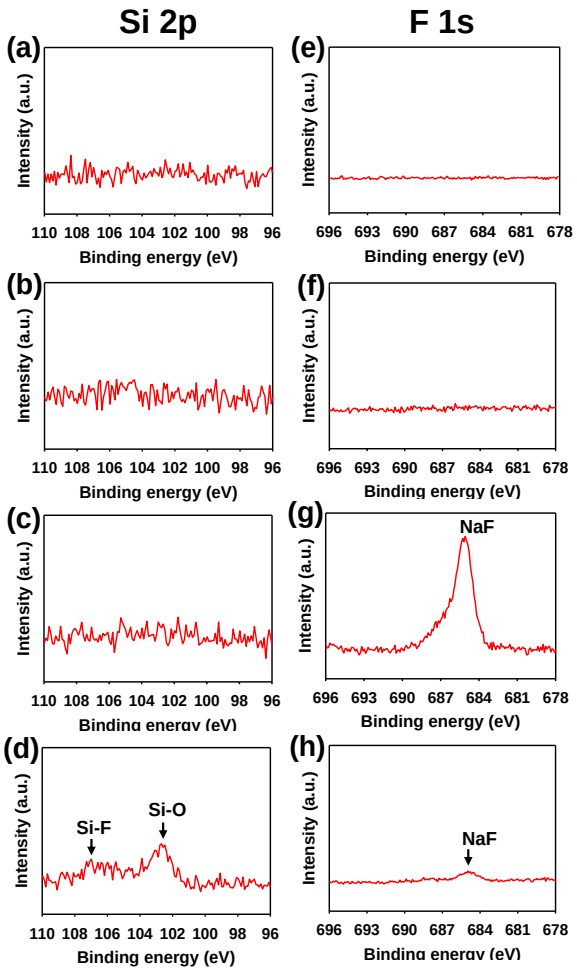

Fig. 6 Si 2p and F 1s 1s XPS spectra of (a,e) pristine Sn_4P_3 anodes and anodes precycled in (b,f) baseline electrolyte, (c,g) FEC-added electrolyte, and (d,h) FEC+TMSP-added electrolyte.

Interestingly, the NaF peak intensity was drastically decreased in the spectrum of the anode cycled in the FEC+TMSP-containing electrolyte. This result suggests that the TMSP additive suppresses the formation of large amounts of NaF by FEC decomposition on the Sn_4P_3 anode. The unique TMSP function of eliminating HF from the FEC additive is proposed in Fig. 7a. This HF removal can reduce NaF formation in the SEI on the Sn_4P_3 anode. In addition, the Si-F moiety can be formed via the reaction of TMSP with HF from FEC, as depicted in Fig. 7a. Moreover, byproducts formed by TMSP decomposition can contribute to the components of the SEI layer. Evidence for the presence of Si-F and Si-O groups in the SEI layer on the anode precycled in the FEC+TMSP-added electrolyte is given in the Si 2p spectra in Fig. 6d. As clearly shown in Figs. 2a,b and 3a, unlike the baseline electrolyte, the FEC-added electrolyte inhibited the formation of the $Na_{15}Sn_4$ phase. This behavior can be explained by the NaF-based SEI generated via the FEC decomposition, as illustrated in Fig. 8. The NaF resistive layer is thought to impede the migration of Na ions into the anode; thus, the formation of the $Na_{15}Sn_4$ phase, which causes a huge volume expansion of Sn_4P_3 anodes, is effectively prevented.

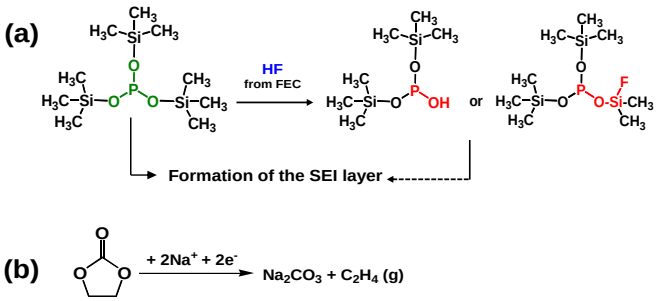

Fig. 7 Schematic of possible mechanisms for (a) a unique function of TMSP scavenging HF from the FEC and contributing to SEI formation on the anode and (b) the electrochemical reaction of EC with Na ions and electrons.

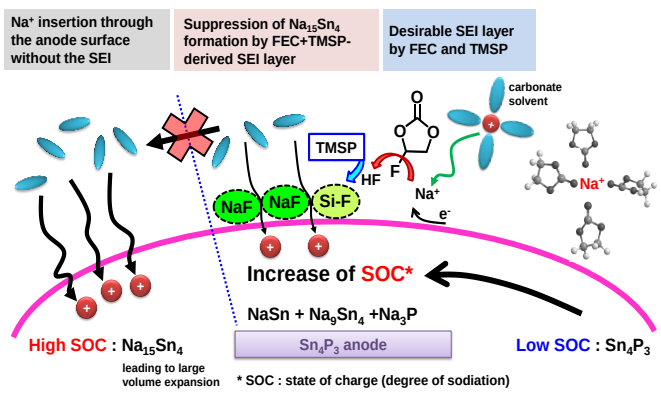

Fig. 8 Schematic showing the function of the NaF-based SEI layer formed during sodiation.

The C 1s XPS spectra in Fig. 9b clearly show that the peaks assigned to the ether (C-O-C) moiety and sodium carbonate (Na_2CO_3) are more intense for the Sn_4P_3 anodes cycled in the baseline electrolyte than for the Sn_4P_3 anodes cycled in the

FEC- and FEC+TMSP-containing electrolytes. The ether and Na_2CO_3 can be generated by EC decomposition (Fig. 7b). This result is in good agreement with the EDS results that strong C, O, and Cl signals formed by the electrolyte decomposition are detected on the anode precycled in the baseline electrolyte. The FEC and TMSP additives effectively prohibit the formation of ether and Na_2CO_3 by EC decomposition, as shown in Figs. 9c,d. In addition, a comparison of the C 1s XPS spectra in Figs. 9b-d indicates that the intensity of the peak corresponding to the C-C of carbon black particles discernibly decreases in the case of the baseline electrolyte. This decrease in the C-C peak intensity is attributed to a very thick surface film formed by the decomposition of the baseline electrolyte; this film blocks the C-C signal from the carbon black particles. This result is consistent with the SEM observation showing the formation of the SEI layer on the carbon black (zone A in Fig. 4b).

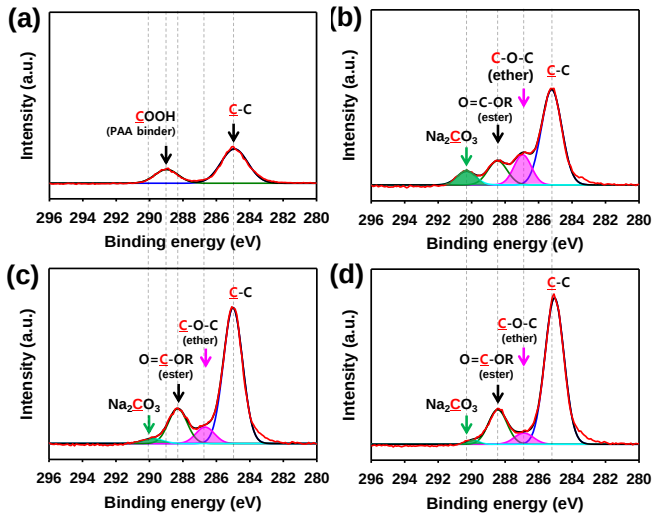

Fig. 9 C 1s XPS spectra of (a) pristine Sn_4P_3 anodes and anodes precycled in (b) baseline electrolyte, (c) FEC-added electrolyte, and (d) FEC+TMSP-added electrolyte.

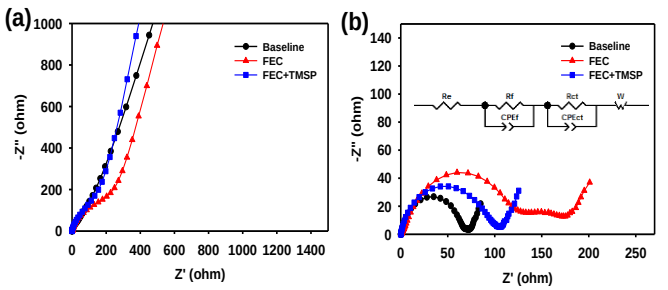

Fig. 10 Electrochemical impedance spectra of Sn_4P_3 anodes (a) before and (b) after full sodiation in baseline electrolyte, FEC-added electrolyte, and FEC+TMSP-added electrolyte. The equivalent circuit, which was used to fit the impedance data, is shown in inset of Fig. 10b.

Fig. 10 shows the electrochemical impedance spectra of Sn_4P_3 anodes before and after full sodiation. The impedance data have been fitted with an ordinary equivalent circuit shown in the inset of Fig. 10b. Fig. 10b presents the contribution to the cell impedance from three components: the intercept at high frequency for the electrolyte resistance (R_e), the impedance (R_f) associated with Li^+ migration across the SEI, and the resistance (R_{ct}) for the faradaic charge transfer reaction at low frequency. Two RC parallel elements in series describe SEI film on the anode surface (R_f and CPE_f) and Li^+ charge transfer at interface (R_{ct} and CPE_{ct}), respectively. The circuit shown in the inset of Fig. 10b includes, in addition, the electrolyte resistance (R_e) and the Warburg impedance (W), which is associated with Li^+ diffusion in Sn_4P_3 particles. A remarkable feature is that the interfacial resistance, including the SEI resistance and charge transfer resistance components, is higher for the Sn_4P_3 anodes with full sodiation in the FEC- and FEC+TMSP-added electrolytes than in the baseline electrolyte (Fig. 10b). The addition of FEC into the baseline electrolyte led to considerable increase in the impedance ascribed to Li-ion migration across the SEI (R_f, 50.5 Ω → 125 Ω) and charge transfer resistance (R_{ct}, 20 Ω → 49 Ω), as presented in Table S1. This implies that the NaF produced by the FEC decomposition acts as a highly resistive layer for charge transport. Interestingly, the semicircle of the Sn_4P_3/Na half-cells with FEC+TMSP after full sodiation was slightly smaller than the corresponding semicircle of the anode in the FEC-added electrolyte. The simulation results of Table S1 clearly show that the SEI resistance (R_f) was reduced from 125 Ω to 91 Ω with the introduction of TMSP in the FEC-added electrolyte. This indicates the facilitation of Li-ion migration through the FEC+TMSP-derived SEI. Moreover, charge transfer resistance (R_{ct}) decreased from 49 Ω to 14 Ω in the FEC+TMSP-added electrolyte (Table S1). This is possibly because the TMSP additive modified the FEC-derived SEI layer mainly composed of resistive NaF. The hybrid SEI layer formed by the decomposition of the binary additive (FEC+TMSP) exhibited relatively high interfacial resistance compared to the baseline electrolyte (Fig. 10b) and thereby the formation of the $Na_{15}Sn_4$ phase showing severe volume expansion during the Na insertion process could be avoided, as depicted in Fig. 8. This finding suggests that the characteristics of the surface layer formed on the Sn_4P_3 anode represent a critically important factor that influences the kinetics of sodiation–desodiation.

Conclusions

We have demonstrated a highly promising approach to creating high-performance Sn_4P_3 anodes for Na-ion batteries. Our investigation revealed that the FEC additive creates a resistive NaF-based SEI that controls the formation of the $Na_{15}Sn_4$ phase, which exhibits severe volume expansion, and that the TMSP additive effectively eliminates HF from the FEC decomposition to mitigate the formation of a large fraction of NaF and to build up more stable and robust SEI layers. Cycling tests of Sn_4P_3 anodes confirmed that robust SEI layers were essential to inhibit unwanted electrolyte decomposition and to preserve the electrochemical properties of metallic anodes. Moreover, possible mechanisms for the surface chemistry of the Sn_4P_3 anode with and without the FEC+TMSP binary additive were

proposed. The baseline electrolyte formed no protective films on the anode, whereas the FEC- and FEC+TMSP-containing electrolytes produced stable SEI layers, thereby preventing aggregation of the Sn_4P_3 particles. These findings and the associated analyses show that the use of a suitable additive is a promising and efficient approach to create high-performance Sn_4P_3 anodes in Na-ion batteries.

Acknowledgements

This research was supported by Korea Electrotechnology Research Institute (KERI) Primary research program through the National Research Council of Science & Technology funded by the Ministry of Science, ICT and Future Planning (MSIP) (No. 14-12-N0101-69) and by a grant from the Energy Efficiency & Resources of the Korea Institute of Energy Technology Evaluation and Planning (Project no. 20112010100140) funded by the Korean Ministry of Knowledge Economy.

Notes and references

[a] School of Energy and Chemical Engineering, Ulsan National Institute of Science and Technology (UNIST) 100 Banyeon-ri, Eonyang-eup, Ulju-gun, Ulsan, 689-798, South Korea. E-mail: ktlee@unist.ac.kr and nschoi@unist.ac.kr

[b] School of Chemical and Biological Engineering, Seoul National University 599 Gwanangno, Gwanak-gu, Seoul 151-744, South Korea.

[c] Battery Research Center, Korea Electrotechnology Research Institute, 12 Bulmosan-ro 10 beon-gil, Changwon 642-120, South Korea.

Electronic Supplementary Information (ESI) available: comparison of cycling performance of the Sn_4P_3 anodes with and without the TMSP additive, simulation results for AC impedance spectra of the Na/Sn_4P_3 cells. See DOI: 10.1039/b000000x/

1 V. Palomares, P. Serras, P. I. Villaluenga, K. B. Hueso, J. Carretero-Gonzalez, and T. Rojo, *Energy Environ. Sci*. 2012, **5**, 5884-5901.

2 H. Pan, Y. -S. Hu and L. Chen, *Energy Environ. Sci*. 2013, **6**, 2338-2360.

3 S. Y. Hong, Y. Kim, Y. Park, A. Choi, N. -S. Choi and K. T. Lee, *Energy Environ. Sci*. 2013, **6**, 2067-2081.

4 M. D. Slater, D. Kim, E. Lee and C. S. Johnson, Adv. Funct. Mater. 2013, **23**, 947-958.

5 S. -W. Kim, D. -H. Seo, X. Ma, G. Ceder and K. Kang, *Adv. Energy Mater*. 2012, **2**, 710- 721.

6 Y. Cao, L. Xiao, W. Wang, D. Choi, Z. Nie, J. Yu, L. V. Saraf, Z. Yang and J. Liu, *Adv. Mater*. 2011, **23**, 3155–3160.

7 X. Liu, X. Wang, A. Iyo, H. Yu, D. Li and H. Zhou, *J. Mater. Chem. A*, 2014, ***2***, 14822–14826.

8 K. H. Ha, S. H. Woo, D. Mok, N. S. Choi, Y. Park, S. M. Oh, Y. Kim, J. Kim, J. Lee, L. F. Nazar and K. T. Lee, *Adv. Energy Mater*. 2013, **3**, 770-776.

9 H. Kim, I. Park, S. Lee, H. Kim, K. -Y. Park, Y. -U. Park, H. Kim, J. Kim, H. -D. Lim, W. -S. Yoon and K. Kang, *Chem. Mater*. 2013, **25**, 3614-3622.

10 Z. Jian, L. Zhao, H. Pan, Y. -S. Hu, H. Li, W. Chen and L. Chen, *Electrochem. Commun*. 2012, **14**, 86-89.

11 Y. -U. Park, D. -H. Seo, H. -S. Kwon, B. Kim, J. Kim, H. Kim, I. Kim, H. -I. Yoo and K. Kang, *J. Am. Chem. Soc*. 2013, **135**, 13870–13878.

12 J. Qian, Y. Chen, L. Wu, Y. Cao, X. Ai and H. Yang, *Chem. Commun*. 2012, **48**, 7070-7072.

13 X. Zhou, Z. Dai, J. Bao and Y.-G. Guo, *J. Mater. Chem. A*, 2013, **1**, 13727-13731.

14 A. Darwiche, C. Marino, M. T. Sougrati, B. Fraisse, L. Stievano and L. Monconduit, *J. Am. Chem. Soc.* 2012, **134**, 20805-20811.

15 J. Qian, X. Wu, Y. Cao, X. Ai and H. Yang, *Angew. Chem., Int. Ed.* 2013, **52**, 4633-4636.

16 Y. Kim, Y. Park, A. Choi, N. -S. Choi, J. Kim, J. Lee, J. H. Ryu, S. M. Oh and K. T. Lee, *Adv. Mater*. 2013, **25**, 3045-3049.

17 W. Li, S. -L. Chou, J. -Z. Wang, J. H. Kim, H. -K. Liu and S. -X. Dou, *Adv. Mater*. 2014, **26**, 4037-4042.

18 Y. Kim, Y. Kim, A. Choi, S. Woo, D. Mok, N. -S. Choi, Y. S. Jung, J. H. Ryu, S. M. Oh and K. T. Lee, *Adv. Mater*. 2014, **26**, 4139-4144.

19 S. Komaba, T. Ishikawa, N. Yabuuchi, W. Murata, A. Ito and Y. Ohsawa, *ACS Appl. Mater. Interfaces*, 2011, **3**, 4165-4168.

20 N. -S. Choi, Y. Yao, Y. Cui and J. Cho, *J. Mater. Chem*. 2011, **21**, 9825-9840.

21 N. -S. Choi, K. H. Yew, K. Y. Lee, M. Sung, H. Kim and S. S. Kim, *J. Power Sources*, 2006, **161**, 1254-1259

22 J. T. Vaughey, J. Owejan and M. M. Thackeray, *Electrochem. Solid-State Lett*. 2007, **10**, A220-A224.

23 J. -J. Zhang, X. Zhang and Y. -Y. Xia, *J. Electrochem. Soc*. 2007, **154**, A7-A13.

24 J. Y. Jang, H. Kim, Y. Lee, K. T. Lee, K. Kang and N. -S. Choi, *Electrochem. Commun*. 2014, **44**, 74–77.

25 L. Ji, M. Gu, Y. Shao, X. Li, M. H. Engelhard, B. W. Arey, W. Wang, Z. Nie, J. Xiao, C. Wang, J. -G. Zhang and J. Liu, *Adv. Mater*. 2014, **26**, 2901-2908.

26 A. Magasinski, B. Zdyrko, I. Kovalenko, B. Hertzberg, R. Burtovyy, C. F. Huebner, T. F. Fuller, I. Luzinov, and G. Yushin, *ACS Applied Mater. & Inter*. 2010, **2**, 3004-3010.

27 L. D. Ellis, T. D. Hatchard and M. N. Obrovac, *J. Electrochem. Soc*. 2012, **159**, A1801-A1805.

28 M. K. Datta, R. Epur, P. Saha, K. Kadakia, S. K. Park and P. N. Kumta, *J. Power. Sources*, 2013, **225**, 316-322.

29 J. Qian, Y. Xiong, Y. Cao, X. Ai and H. Yang, *Nano Lett*. 2014, **14**, 1865-1869.

30 Q. Shen, J. Li and L. Zhang, *Solar Energy Materials and Solar Cells*, 2000, **62**, 167-172.

A table of contents entry

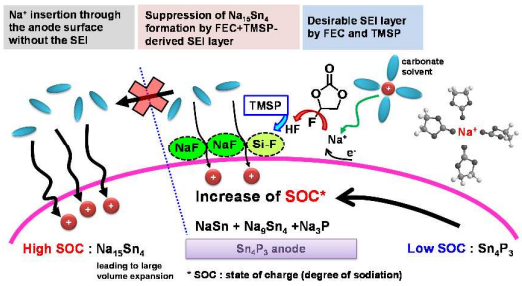

Interfacial architectures based on the FEC+TMSP binary additive prevent the formation of $Na_{15}Sn_4$ with severe volume expansion and electrolyte decomposition.